Journal of Physics: Conference Series **579** (2015) 012008 doi:10.1088/1742-6596/579/1/012008

Numerical investigation of a high head Francis turbine under steady operating conditions using foam-extend

M. Lenarcic, M. Eichhorn, S. J. Schoder and Ch. Bauer

Institute for Energy Systems and Thermodynamics, Vienna University of Technology, Getreidemarkt 9, 1060 Vienna, Austria

E-mail: markus.lenarcic@tuwien.ac.at

Abstract.

In this work the incompressible turbulent flow in a high head Francis turbine under steady operating conditions is investigated using the open source CFD software package FOAM-extend-3.1. By varying computational domains (cyclic model, full model), coupling methods between stationary and rotating frames (mixing-plane, frozen-rotor) and turbulence models ($k\omega$-SST, $k\epsilon$), numerical flow simulations are performed at the best efficiency point as well as at operating points in part load and high load. The discretization is adjusted according the y^+-criterion with $y^+_{mean} > 30$. A grid independence study quantifies the discretization error and the corresponding computational costs for the appropriate simulations, reaching a GCI $< 1\%$ for the chosen grid. Specific quantities such as efficiency, head, runner shaft torque as well as static pressure and velocity components are computed and compared with experimental data and commercial code. Focusing on the computed results of integral quantities and static pressures, the highest level of accuracy is obtained using FOAM in combination with the full model discretization, the mixing-plane coupling method and the $k\omega$-SST turbulence model. The corresponding relative deviations regarding the efficiency reach values of $\Delta\eta_{rel} \sim 7\%$ at part load, $\Delta\eta_{rel} \sim 0.5\%$ at best efficiency point and $\Delta\eta_{rel} \sim 5.6\%$ at high load. The computed static pressures deviate from the measurements by a maximum of $\Delta p_{rel} = 9.3\%$ at part load, $\Delta p_{rel} = 4.3\%$ at best efficiency point and $\Delta p_{rel} = 6.7\%$ at high load. Commercial code in turn yields slightly better predictions for the velocity components in the draft tube cone, reaching a good accordance with the measurements at part load. Although FOAM also shows an adequate correspondence to the experimental data at part load, local effects near the runner hub are captured less accurate at best efficiency point and high load. Nevertheless, FOAM is a reasonable alternative to commercial code that makes it possible to predict integral quantities and local parameters under steady operating conditions adequately.

1. Introduction

Numerical flow simulations are still the most applicable way for determining the operating conditions of hydraulic machines. Keck et al. [1] chronologically recapitulate the main steps of ordinary CFD towards its specific application in turbomachinery by implementing rotor-stator coupling methods like mixing-plane and frozen-rotor interfaces. In this context, the open source CFD software package OpenFOAM® is noted, which was commercialized and distributed by NABLA Ltd. from 2000 till 2004 [2]. Since then, a lot of effort has been applied in adapting and generating necessary features for turbomachinery purposes. The corresponding main interests

and extensions in this field are still coordinated by the OpenFOAM® Turbomachinery Working Group [3], which continuously organizes workshops to forward appropriate code innovations [4]-[7]. The implementation of the General Grid Interface (GGI), the mixing-plane approach as well as the frozen-rotor coupling method is described in [8]-[9] and part of the new release called FOAM-extend-3.1 [10]. The capabilities of this mixing-plane coupling method are investigated in [11], wherein the computed results correlate well with the expected main flow characteristics. Further CFD simulations in hydraulic turbines have been carried out with OpenFOAM® in [12]-[15].

In order to evaluate the accuracy of state-of-the-art CFD simulations under steady operating conditions, the first Francis-99 workshop has been introduced by the NTNU in Trondheim. Therefore, appropriate measurements at different operating points were provided, which prescribe the numerical boundary conditions, validate the computed results and reveal the current possibilities of numerics and powerful computers. The investigated hydraulic machine is a scaled down model of Tokke power plant in Norway - the associated test rig is located at the NTNU. The model consists of 14 stay vanes (including two different types) embedded inside a spiral case, 28 guide vanes, a runner with 15 splitter and 15 full length blades and an elbow draft tube. Measurements have been carried out at part load (PL), best efficiency point (BEP) and high load (HL) with different guide vane angles, discharges and rotational speeds. Steady-state as well as unsteady flow simulations have already been done on this model by Trivedi et al. [16] and Moritz [17], leading to good agreements with experimental data at BEP and HL but to significant differences at PL. Based on these publications, further numerical investigations have to be performed. The corresponding conditions are summarized in table 1, which promote the validation of numerical simulations over a wide range of possible turbine operating conditions.

Table 1. Operating conditions proposed for the Francis-99 workshop; Operating conditions for the LDA measurements (*)

Objective	Unit	PL	BEP	HL	$\text{PL}^\star_{\text{LDA}}$	$\text{BEP}^\star_{\text{LDA}}$	$\text{HL}^\star_{\text{LDA}}$
H	m	12.290	11.910	11.840	12.290	12.77	12.61
Q	m^3/s	0.071	0.203	0.221	0.071	0.21	0.23
n	1/s	6.770	5.590	6.160	6.770	5.74	6.34
α	deg	3.910	9.840	12.440	3.910	9.84	12.44
η_M	%	71.690	92.610	90.660	72.500	92.40	91.00
T	Nm	137.520	619.560	597.990	-	-	-
ρ	kg/m^3	999.230	999.190	999.200	999.230	999.19	999.20

In the course of this work, numerical flow simulations of the mentioned scaled down model are done using FOAM-extend-3.1 and commercial code. The geometry is spatially discretized with Ansys ICEM® 15.0 according to the y^+-criterion with $y^+_{mean} > 30$ and composed to a cyclic model and a full 360° model with integrated spiral case (see section 3.2). Effects of different turbulence models ($k\omega$-SST, $k\epsilon$) and coupling methods at the interfaces between stationary and rotating frames (mixing-plane, frozen-rotor) are outlined as well.

Various integral quantities such as the head, efficiency and runner torque as well as static pressure and velocity components are computed and compared with experimental data. Therefore, pressure measurements have been performed at six different locations in the vaneless space, the runner and the draft tube (see figure 1). Furthermore, LDA measurements for the axial- and circumferential velocity components have been done at several points along two horizontal lines in the draft tube cone (see table 2). The relative positions of the pressure

sensors P41, P71 and S51 are fixed within the runner domain, rotating with the appropriate rotational speed n.

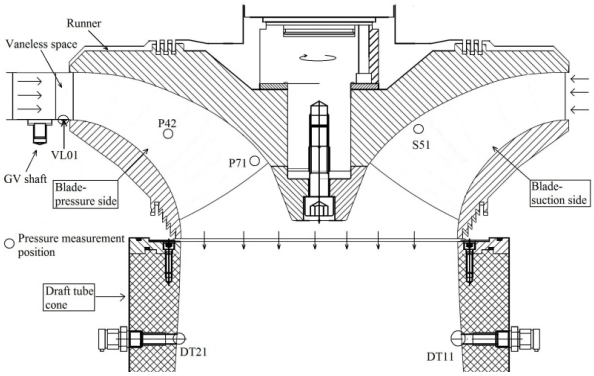

Figure 1. Monitoring points of the experimental pressure measurements [18]

Table 2. Cartesian coordinates of LDA monitoring points

Coord.	Unit	Top Line		Bottom Line	
-	-	Start	End	Start	End
x	mm	0	-178.9	0	-196.5
y	mm	0	0	0	0
z	mm	-243.4	-243.4	-561.4	-561.4

2. Numerical Setup

The computational domain includes all relevant components between spiral case inlet and draft tube outlet, whereby the distance between inlet and actual model is chosen sufficiently large in order to keep the influence of the boundary condition moderate. Stationary parts like spiral case (SC), stay vanes (SV) and guide vanes (GV) are connected to each other by General Grid Interfaces (GGI). The numerical couplings between guide vanes, runner (RN) and draft tube (DT) are achieved by mixing-plane and frozen-rotor approaches respectively.

A constant discharge is set as inlet boundary condition for full models and a corresponding velocity distribution with an incidence angle of $\beta = 9°$ is prescribed for cyclic models. The turbulent quantities are computed by specifying a turbulent intensity of $I = 0.05$ and a uniform turbulent mixing length of $l_t = 0.01m$. In order to consider rotational effects of the runner, a constant rotational speed is defined depending on the appropriate operating conditions. A so-called opening boundary condition with a prescribed value for the mean static pressure enables a re-entering flow and reduces numerical oscillations at the outlet. Values of discharge and rotational speed are set according to table 1. Considering an incompressible single phase flow based on the Reynolds-averaged Navier-Stokes (RANS) method, steady operating conditions are prescribed for all numerical simulations. Convective terms are approximated by 2^{nd}-order interpolation schemes. The maximum number of iteration steps is limited by an abortion criterion for the absolute values of residuals and the evaluated quantities are averaged over a certain iteration step period. In order to improve the numerical stability during the calculation process, moderate under-relaxation factors are chosen. The SIMPLE-algorithm executes the steady-state pressure-velocity coupling in FOAM, whereas commercial code in turn uses a fully coupled solver. With regard to the mixing-plane approach integrated in FOAM, pressure and velocity components are area-averaged at the interface, whereas the turbulence quantities are flux-averaged. Commercial code operates with a constraint of constant total pressure on both sides of the interface. But unless otherwise noted, the computed results are obtained with FOAM using the mixing-plane approach and the kω-SST turbulence model.

3. Discretization

3.1. Grid independence study and quality

In order to quantify the discretization error, a grid independence study is carried out using the full model at three different grid refinements ($h_i = 1, 1.3, 1.7$). Therefore, the efficiency η is

computed with commercial code at BEP and compared with an estimated value $f_{h_i=0}$ from the Richardson Extrapolation [19]:

$$f_{h_i=0} \approx f_{h_i=1} + \frac{f_{h_i=1} - f_{h_i=1.3}}{r^p - 1} \tag{1}$$

Therein, $f_{h_i=1,1.3}$ are the computed values, r represents the grid refinement with a value of $r \geq 1.3$ according to [20] and p is the formal order of accuracy. Referring to this equation, the value of the quantity $f_{h_i=0}$ can be approximated if the normalized grid spacing h_i approaches zero. The corresponding data set is given in table 3 and figure 2, where a monotonic convergence regime is clearly visible.

Table 3. Normalized efficiency η as quantity of f_{h_i}

Grid	h_i	r	$f_{h_i}/f_{h_i=1.7}$
-	-	-	-
Fine	1.0	1.3	0.995
Mean	1.3	1.3	0.997
Coarse	1.7	-	1.000

Table 4. Grid Convergence Index (GCI) at different mesh refinements

ϵ_{21}	ϵ_{32}	p	GCI_{21}	GCI_{32}
-	-	-	%	%
0.2	0.3	1.57	0.52	0.79

The Grid Convergence Index (GCI) represents an empirical error band around the asymptotic numerical value. The GCI of the fine grid is defined as

$$GCI_{21} = \frac{F_s|\epsilon_{21}|}{r^p - 1} \tag{2}$$

and the GCI of the coarse grid as $GCI_{32} = F_s|\epsilon_{32}|r^p/(r^p - 1)$. The safety factor is assumed with $F_s = 1.25$ according to [21]. The computed results of the grid independence study show for either GCI comparatively small deviations from the asymptotic value (see table 4).

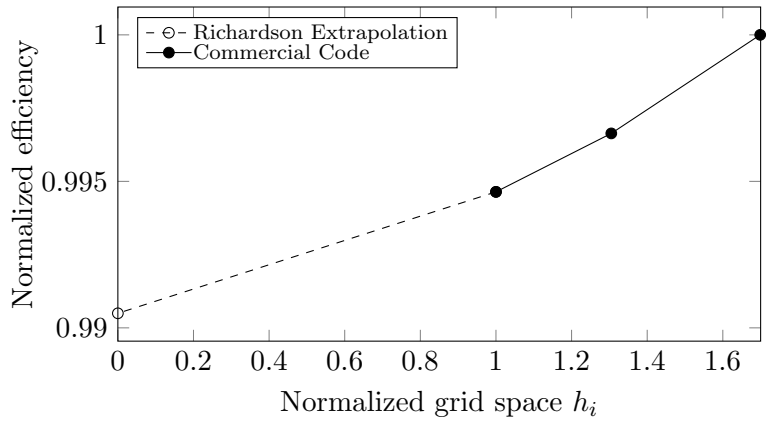

Figure 2. Computed normalized efficiency at three different grid refinements ($h_i = 1, 1.3, 1.7$) using commercial code with the full model; Comparison with the asymptotic estimation from the Richardson Extrapolation

Focusing on computational costs and the level of accuracy, the hexahedral coarse grid ($h_i = 1.7$) is chosen as reference grid. A summary of the corresponding grid quality is given in table 5. The standard wall function, as a suitable compromise between computational time and numerical accuracy, is considered for all further computations. as long as the dimensionless wall distance exceeds values of $y^+ > 30$.

Table 5. Grid quality; Quantities are averaged from SV type 1 and SV type 2 integrated in the spiral case (*)

Objective	Unit	SC	SV*	GV	RN	DT
Min. Determinant	-	0.41	0.35	0.36	0.18	0.66
Min. Angle	deg	14	23	21	11	42
y^+_{mean}	-	> 30	> 30	> 100	> 100	> 100

3.2. Physical models
The influence of the computational domains on the computed results are carried out by considering two different types of physical models: A cyclic model with a simplified extension of the inlet domain, which includes the whole 360° geometry except the spiral case (see figure 3) and a full model, which represents the spatial discretization of the entire hydraulic machine with an extension of the inlet domain at the spiral case (see figure 4).

Table 6. Composition of the physical models and their total number of nodes

Model	SC	SV Type 1	SV Type 2	GV	RN	DT	Total Number of Nodes
-	-	-	-	-	-	-	10^6
Cyclic	-	180°	180°	360°	360°	360°	4.3
Full	360°	180°	180°	360°	360°	360°	4.2

Detailed information about the model compositions and their total number of nodes can be seen in table 6.

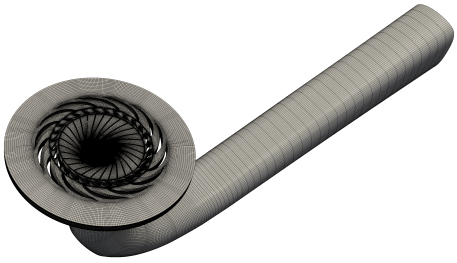

Figure 3. Cyclic model

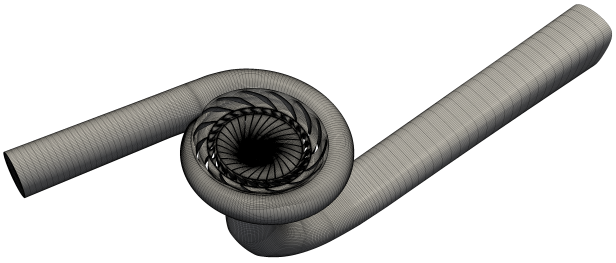

Figure 4. Full model

4. Results
By varying computational domains, coupling methods between stationary and rotating frames, turbulence models and solvers, numerical flow simulations are performed for the operating points PL, BEP and HL. The prescribed operating conditions and monitoring points are given in table 1 and table 2. Regarding the results, table 7 and table 8 illustrate the relative deviations of the computed integral quantities and static pressure results with the corresponding measurements. The evaluation of the velocity components are shown from figure 5 to figure 10. Therein, a radius ratio of $r/r_0 = 0$ represents the starting point on the rotational axis and $r/r_0 = 1$ the end point at the draft tube wall.

4.1. Cyclic models

Table 7 shows the relative deviations between computed results and experimental data concerning the integral quantities and the static pressures. By considering the cyclic model it can be seen that FOAM yields a high level of accuracy at all investigated operating points. Since the mixing-plane interface causes significant differences at PL concerning the runner shaft torque ($\Delta T_{rel} \sim 37\%$), the frozen-rotor coupling method has been additionally applied to evaluate the influence of either approach. Despite of reaching comparable values for the static pressure and the head H, the runner shaft torque is differently captured and more precise using the frozen-rotor interface. This can be lead back to the underlying mathematical algorithm and the different treatment of simplified mass transfer at this specific operating condition. However, the computed results obtained with commercial code are slightly affected by the different types of coupling methods, except for the runner shaft torque at PL. So by comparing the computed results with the measurements, FOAM yields the best agreement using frozen-rotor and - despite of the significant discrepancy at PL - acceptable results using the mixing-plane coupling method. Although commercial code predicts the integral quantities more or less insufficiently, the computed values for the static pressure are comparable with those obtained with FOAM.

Table 7. Relative deviations of integral quantities and static pressure between computed results and measurements using the cyclic model, the $k\omega$-SST turbulence model, FOAM/commercial code (CC) and the mixing-plane (MP)/frozen-rotor (FR) coupling method

OP	Config	Unit	H	T	η	VL01	DT11	DT21	P42	P71	S51
PL	FOAM, MP	%	0.9	-36.8	-28.8	0.7	1.3	1.6	11.2	8.0	6.4
	FOAM, FR	%	0.6	13.3	5.3	2.8	0.1	0.4	11.8	5.5	6.0
	CC, MP	%	13.4	19.3	3.7	2.4	-1.8	-1.7	8.5	11.7	4.5
	CC, FR	%	14.1	28.0	8.7	3.4	-1.8	-1.7	8.8	11.8	3.9
BEP	FOAM, MP	%	3.7	1.2	-3.0	1.2	-2.6	-2.2	4.3	3.8	3.0
	FOAM, FR	%	4.4	2.9	-2.2	2.1	-2.6	-2.2	4.3	3.7	3.1
	CC, MP	%	19.8	13.4	-4.4	5.3	-2.6	-2.2	3.9	1.4	8.0
	CC, FR	%	19.5	13.9	-3.9	4.6	-2.5	-2.1	3.8	1.5	8.4
HL	FOAM, MP	%	1.4	-6.9	-7.8	-0.4	-1.7	-0.9	6.3	5.1	3.7
	FOAM, FR	%	1.3	-0.6	-2.1	-0.6	-1.8	-1.0	7.2	4.9	3.7
	CC, MP	%	13.7	8.5	-3.4	-0.7	-7.3	-6.5	2.4	-3.6	4.4
	CC, FR	%	13.2	8.1	-3.4	-1.2	-7.3	-6.5	2.6	-3.5	4.3

The computed velocity components at PL show an adequate correspondence to the measurements for both the axial velocities c_w and the circumferential velocities c_θ (see figure 5), whereas enhanced differences occur at the draft tube wall. Those discrepancies are attributable to the applied standard wall function, which limits the accuracy when the flow condition differs too much from the ideal one and large gradients of physics occur in the boundary layer. However, the computed results at BEP and HL are more or less comparable, showing the maximum deviations near the runner hub, where existing flow structures are not captured well (see figure 6 and figure 7). But although discharge and swirl are incorrectly predicted in this region, the experimental data are mainly reproduced yet. A comparison between the computed velocities obtained with both solvers and coupling methods shows no clear preference, since the quantities are qualitatively similar. But, the accuracy tends to decrease when the mixing-plane approach is applied with FOAM, whereas using the frozen-rotor coupling method yields an adequate correspondence to the measurements.

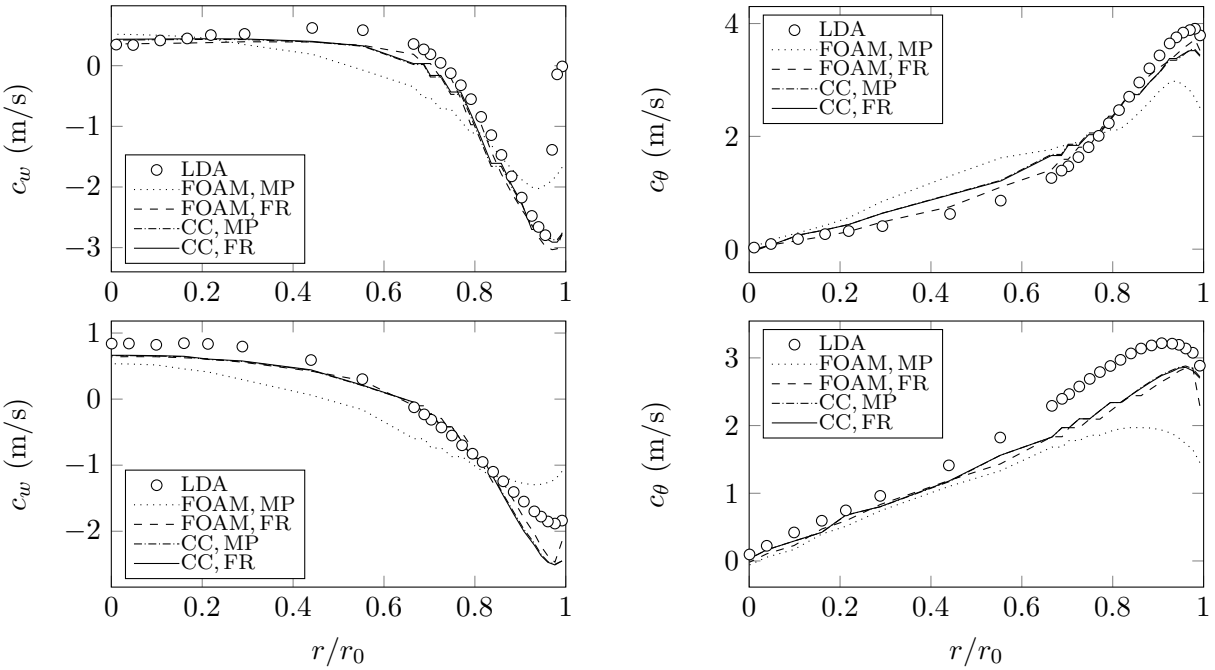

Figure 5. Axial velocity (left) and circumferential velocity (right) on the top line (top) and the bottom line (bottom) at operating point PL using the cyclic model, the kω-SST model, FOAM/commercial code (CC) and the mixing-plane (MP)/frozen-rotor (FR) coupling method

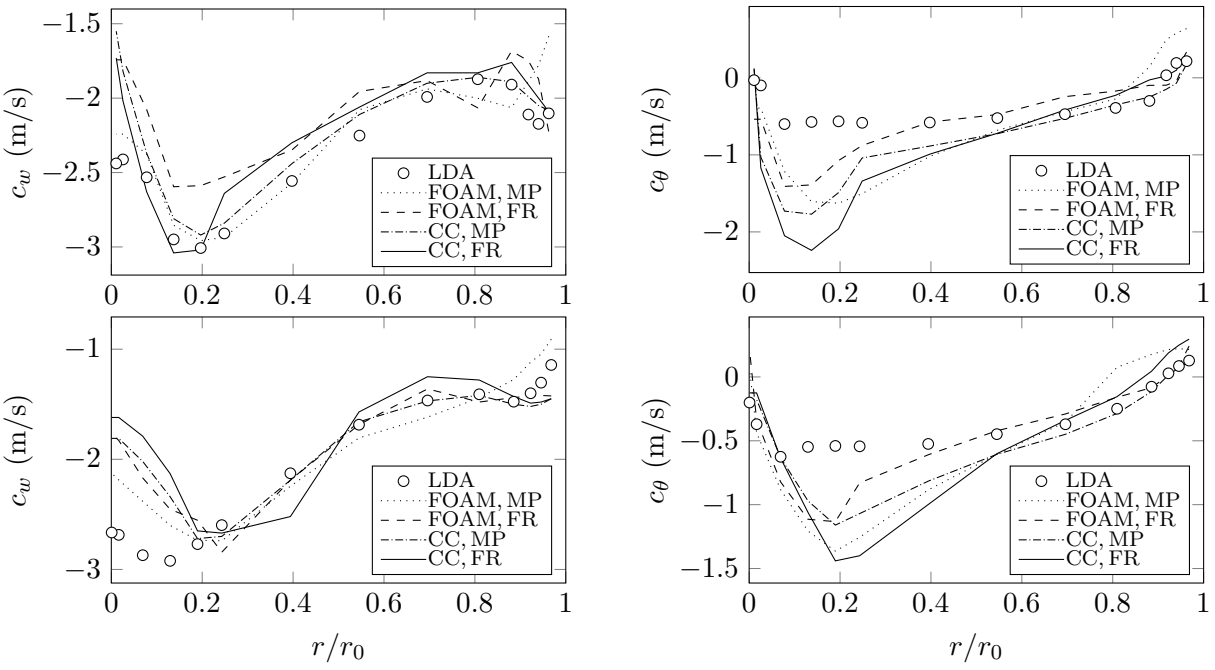

Figure 6. Axial velocity (left) and circumferential velocity (right) on the top line (top) and the bottom line (bottom) at operating point BEP using the cyclic model, the kω-SST model, FOAM/commercial code (CC) and the mixing-plane (MP)/frozen-rotor (FR) coupling method

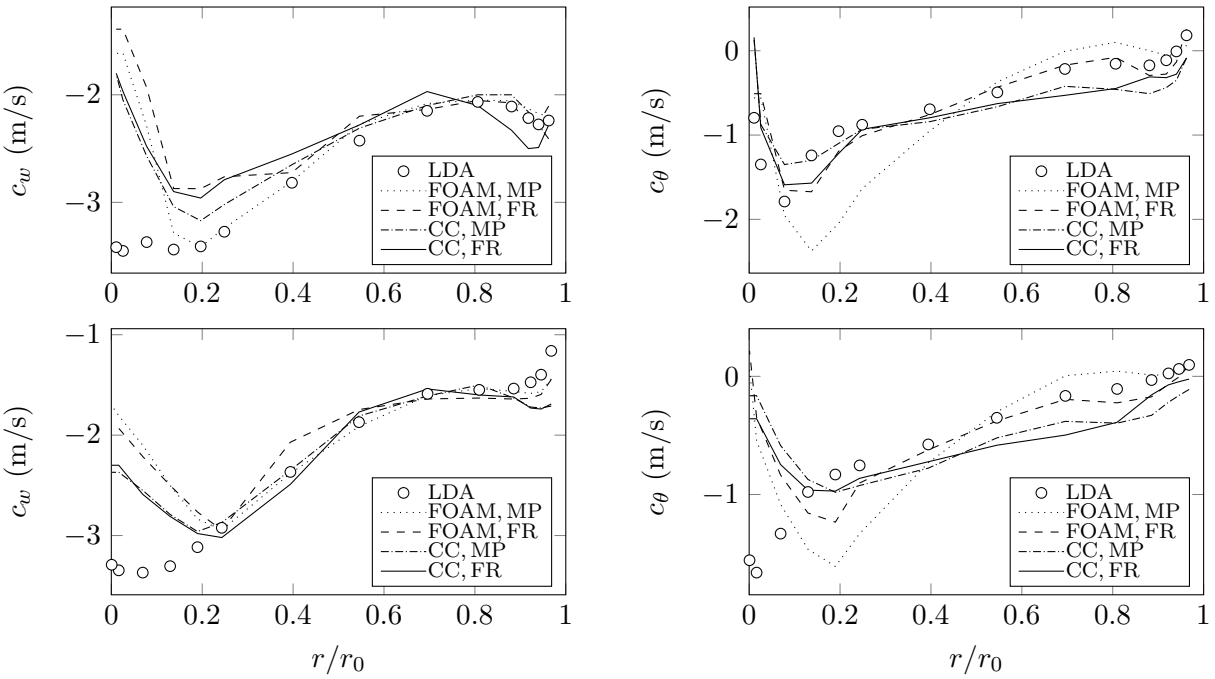

Figure 7. Axial velocity (left) and circumferential velocity (right) on the top line (top) and the bottom line (bottom) at operating point HL using the cyclic model, the kω-SST model, FOAM/commercial code (CC) and the mixing-plane (MP)/frozen-rotor (FR) coupling method

4.2. Full models

Table 8 illustrates the relative deviations between computed results and measurements regarding integral quantities and static pressures. Therefore, the $k\omega$-SST and the $k\epsilon$ turbulence models are applied using the full model with both coupling methods. Considering the frozen-rotor interface does not significantly improve the accuracy, so the corresponding results are not further discussed in this work. Nevertheless, the computed results obtained with FOAM and the $k\omega$-SST turbulence model show a high accuracy concerning the integral quantities at BEP and even adequate values at HL and PL. Compared to the computed results using the cyclic model, considering the full model yields a higher precision regarding the head H at BEP and regarding the runner shaft torque T at PL - the corresponding values are similar at HL. Using the full model positively affects the computation of the integral quantities, which can be lead back to the possibility of considering an affected incident flow as consequence of the different operating conditions. Using the $k\epsilon$ turbulence model with FOAM leads to significant deviations between numerics and experimental data at each operating point, whereas an improving trend is evident when using commercial code. This can be attributed to its underlying numerics and wall treatment, preventing a high level of accuracy in appearance of complex flow structures and near-wall effects. Generally, the head H is computed more precise than the runner shaft torque T. This fact can be lead back to the simplified mass transfer at the interfaces between stationary and rotating frames, which directly influences the computation of the runner shaft torque. On the other hand, the head is calculated at the domain boundaries and thus less affected by mathematical limitations of the coupling methods. Nevertheless, the static pressures are accurately observed using both solvers and turbulence models, reaching a maximum deviation of $\Delta p_{rel} < 12\%$ in the runner domain at PL.

Table 8. Relative deviations of integral quantities and static pressure between computed results and measurements using the full model, the $k\omega$-SST/$k\epsilon$ turbulence model, FOAM/commercial code (CC) and the mixing-plane (MP)/frozen rotor (FR) coupling method

OP	Config	Unit	H	T	η	VL01	DT11	DT21	P42	P71	S51
PL	FOAM, SST, MP	%	-1.4	-6.7	-7.0	3.1	0.2	0.5	9.3	6.6	5.4
	FOAM, SST, FR	%	1.1	14.0	5.4	1.9	-1.2	-0.7	10.5	4.9	5.3
	FOAM, kϵ, MP	%	-7.5	-27.3	-18.0	-1.2	-2.4	-1.9	8.4	7.0	3.3
	CC, SST, MP	%	11.9	16.7	3.0	1.7	-1.8	-1.7	8.4	11.7	4.2
	CC, kϵ, MP	%	9.7	10.3	0.4	1.8	-0.9	-0.9	7.8	9.6	4.1
BEP	FOAM, SST, MP	%	0.6	1.9	0.5	1.3	-2.6	-2.1	4.3	3.8	3.2
	FOAM, SST, FR	%	1.5	3.2	0.8	2.2	-2.7	-2.2	4.3	3.8	3.2
	FOAM, kϵ, MP	%	-2.4	-16.1	-13.7	3.4	-2.8	-2.3	4.3	3.6	3.0
	CC, SST, MP	%	12.2	12.5	0.9	5.1	-2.6	-2.2	3.9	1.5	7.9
	CC, kϵ, MP	%	8.4	7.4	-0.3	3.8	-2.6	-2.2	3.8	1.4	7.8
HL	FOAM, SST, MP	%	-1.8	-7.5	-5.6	-0.5	-1.9	-1.0	6.7	5.0	3.8
	FOAM, SST, FR	%	-1.8	-0.5	0.8	-0.5	-1.8	-0.9	7.3	4.9	3.8
	FOAM, kϵ, MP	%	-3.1	-19.4	-15.7	-2.1	-2.1	-1.2	4.6	5.0	3.4
	CC, SST, MP	%	4.5	6.9	2.8	-1.6	-7.3	-6.5	2.5	-3.7	4.5
	CC, kϵ, MP	%	2.2	3.0	1.5	-2.6	-7.3	-6.5	2.4	-3.8	4.5

The computed axial velocities (c_w) reveal an adequate accordance with the measurements at PL (see figure 8), predicting a vortex formation, which mainly blocks the flow in the core region of the draft tube. The observed swirl increases towards the draft tube wall, resulting in a high level of circumferential velocities (c_θ). The computed flow distribution agrees well with the measurements, even the drop towards the wall is predicted by the numerics. The only exception to this is using the combination of FOAM and the $k\epsilon$ turbulence model, which insufficiently computes swirl and near-wall physics. The corresponding results correlate with an almost swirl-free flow distribution in the draft tube core region, reaching a maximum value for both velocity components at the wall. As mentioned before, the observed deviations at the wall can be attributed to the applied standard wall function, which limits the accuracy of the physics in the boundary layer. At BEP, the computed axial- and circumferential velocities agree well with the measurements above a radius ratio of $r/r_0 \sim 0.2$, but continuously deviate towards the hub (see figure 9). Thereby, a hub vortex is computed, leading to an enhanced swirl at a radius ratio of $r/r_0 \sim 0.2$ and to a reduced discharge towards the hub. But since the measurements show an moderate swirl and an increased discharge at the hub, the local effects in this region are not well captured by the numerics. Nevertheless, the observed near-wall physics are in an adequate accordance with the measurements, except of using FOAM with the $k\epsilon$ turbulence model. The computed results at HL are qualitatively similar to those at BEP, since the discharge at the hub is also insufficiently predicted by the numerics (see figure 10). The circumferential component is observed in an accurate manner but using FOAM with the $k\omega$-SST model leads to significant deviations at a radius ratio of $r/r_0 \sim 0.2$.

A comparison between the computed velocities obtained with both solvers and both turbulence models shows a slight preference for commercial code, particularly at BEP and HL. The observed results vary more according to the applied turbulence model using FOAM than commercial code, which can be lead back to the underlying numerics with its implemented damping functions and smoothing algorithms.

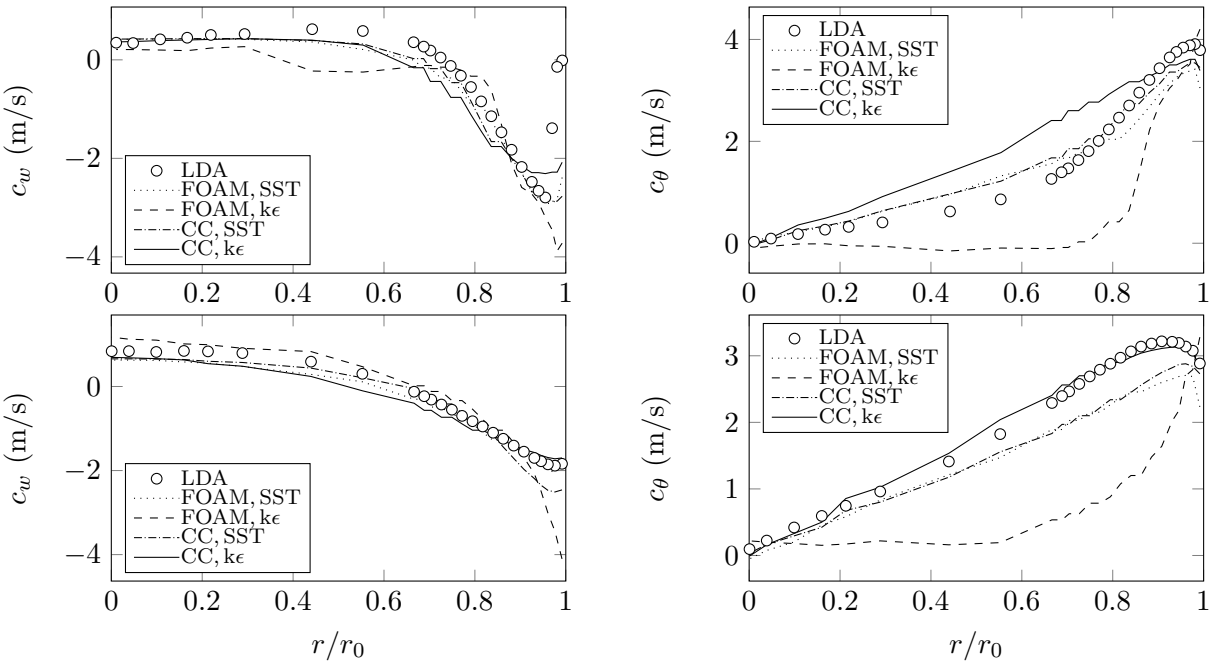

Figure 8. Axial velocity (left) and circumferential velocity (right) on the top line (top) and the bottom line (bottom) at operating point PL using the full model, the kω-SST/kϵ turbulence model, FOAM/commercial code (CC) and the mixing-plane coupling method

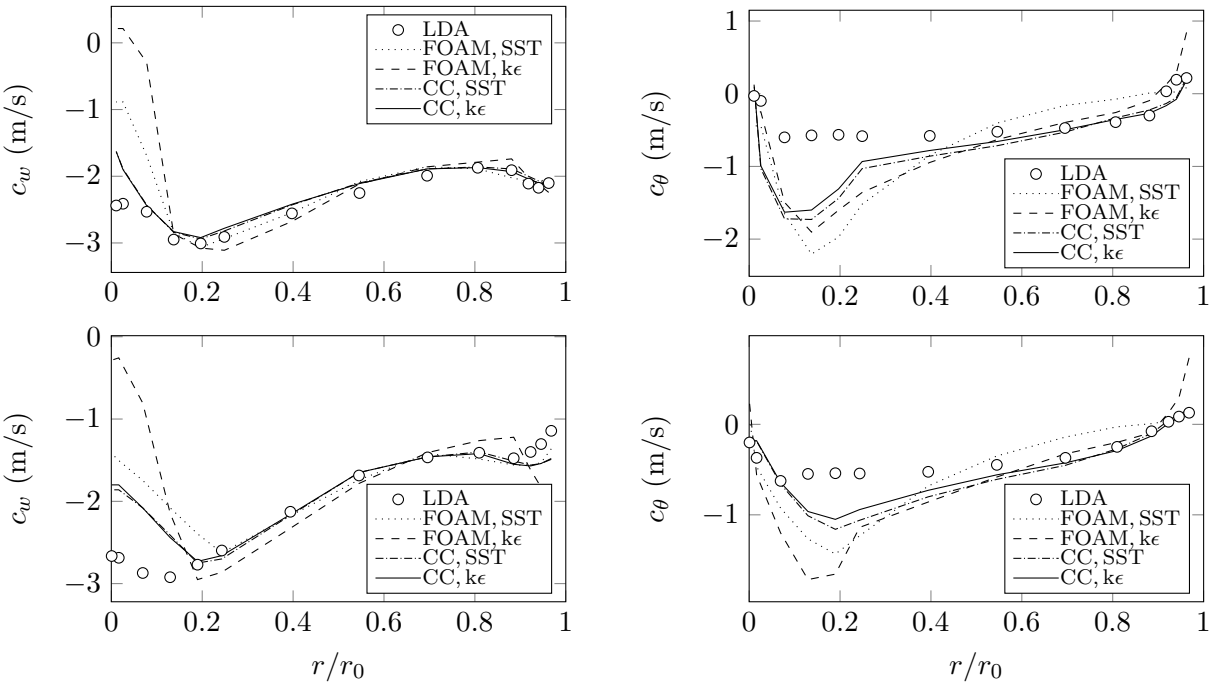

Figure 9. Axial velocity (left) and circumferential velocity (right) on the top line (top) and the bottom line (bottom) at operating point BEP using the full model, the kω-SST/kϵ turbulence model, FOAM/commercial code (CC) and the mixing-plane coupling method

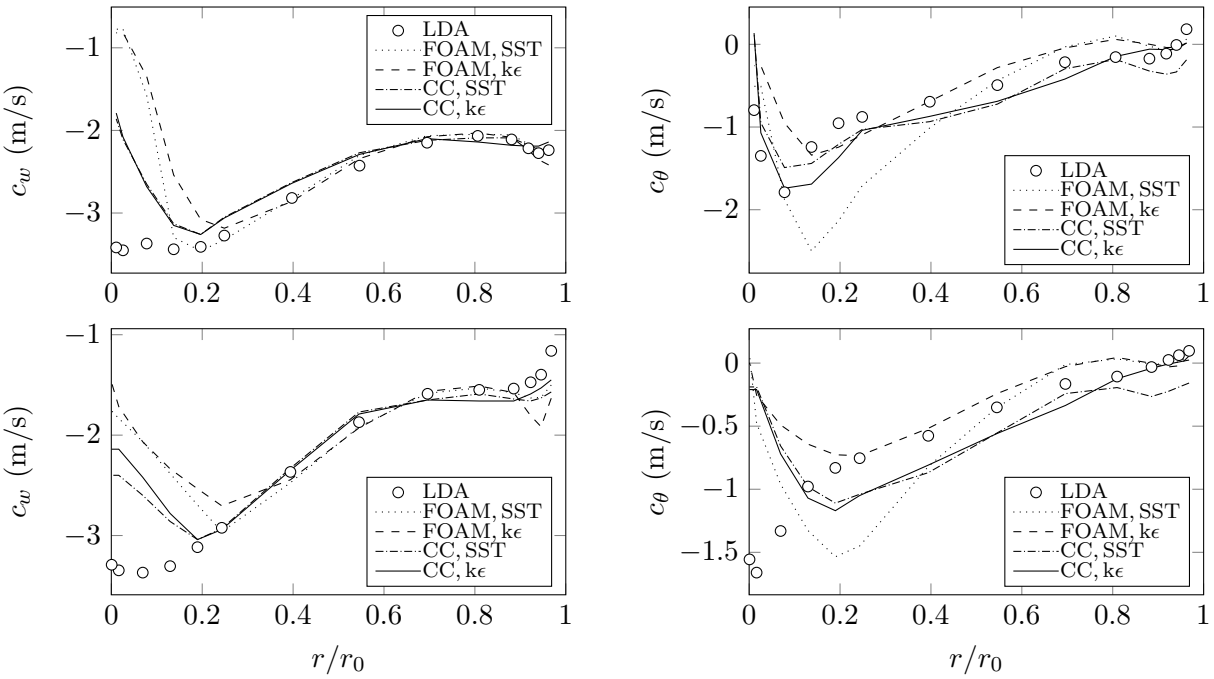

Figure 10. Axial velocity (left) and circumferential velocity (right) on the top line (top) and the bottom line (bottom) at operating point HL using the full model, the kω-SST/$k\epsilon$ turbulence model, FOAM/commercial code (CC) and the mixing-plane coupling method

5. Conclusion

An incompressible turbulent flow in a high head Francis turbine under steady operating conditions is computed using FOAM-extend-3.1. Influences of computational domains (cyclic model, full model), coupling methods (mixing-plane, frozen-rotor), turbulence models (kω-SST, kϵ) and solvers (FOAM, commercial code) are carried out and compared with experimental data of integral quantities, static pressures and velocity components. Therefore, pressure measurements have been done at different locations in the vaneless space, the runner and the draft tube. LDA measurements for the axial- and circumferential velocity components in turn have been performed at several points along two horizontal lines in the draft tube cone. The geometry is spatially discretized and composed both to a cyclic model with a simplified inlet domain and to a full 360° model with an integrated spiral case. The grid refinement is adjusted according to the y^+-criterion with $y^+_{mean} > 30$. A grid independence study is done, resulting in a GCI $< 1\%$ for the chosen computational grid.

At first, numerical flow simulations are performed using the cyclic model with both solvers, coupling methods and the kω-SST turbulence model. Thereby, the frozen-rotor coupling method yields an adequate correspondence to the measurements with deviations of $\Delta\eta_{rel} \sim 5\%$ at part load, $\Delta\eta_{rel} \sim 2\%$ at best efficiency point and $\Delta\eta_{rel} \sim 2\%$ at high load. The corresponding ranges of the static pressures are $\Delta p_{rel} \leq 11.8\%$ at part load, $\Delta p_{rel} \leq 4.3\%$ at best efficiency point and $\Delta p_{rel} \leq 7.2\%$ at high load. On the other hand, using the mixing-plane interface negatively affects the computation of the runner torque at part load and high load, although the head H is well predicted by the numerics. As consequence, the relative deviations of the efficiency increase to a level of $\Delta\eta_{rel} \sim 29\%$ at part load, to $\Delta\eta_{rel} \sim 3\%$ at best efficiency point and to $\Delta\eta_{rel} \sim 8\%$ at high load, whereas the deviations concerning the static pressures are similar to those obtained with the frozen-rotor coupling method. Since those differences are insufficient for predicting such flow parameters, further investigations are done using the full

model with different turbulence models. Applying FOAM with the kϵ turbulence model results in enhanced deviations between the computed efficiency and experimental data, reaching values of $\Delta\eta_{rel} = 18\%$ at part load, $\Delta\eta_{rel} \sim 14\%$ at best efficiency point and $\Delta\eta_{rel} \sim 16\%$ at high load.

With focus on the results computed with FOAM, the highest level of accuracy is obtained using a combination of full model, mixing-plane coupling method and kω-SST turbulence model, since the frozen-rotor interface does not achieve a significant improvement in results when the full model is applied. The consideration of the full 360° discretization particularly improves the flow prediction at part load, where the flow field is characterized by an uneven incident flow and by attached flow regimes. The divergences of the computed static pressures to the experimental data are in an acceptable range at part load ($\Delta p_{rel} \leq 9.3\%$), best efficiency point ($\Delta p_{rel} \leq 4.3\%$) and high load ($\Delta p_{rel} \leq 6.7\%$). Therein, the maximum differences are observed in the runner domain, where complex flow phenomena exist and quantities are directly affected by the simplified mass transfer through the interfaces between stationary and rotating frames. The computed efficiencies show relative deviations of $\Delta\eta_{rel} \sim 7\%$ at part load, $\Delta\eta_{rel} \sim 0.5\%$ at best efficiency point and $\Delta\eta_{rel} \sim 5.6\%$ at high load. Comparing the computed results obtained with either solver, FOAM reaches a higher accuracy regarding the integral quantities and similar values regarding the static pressures.

The computed velocity components show an adequate correspondence to the measurements, although local effects near the runner hub are not fully captured at BEP and HL. Especially the flow regime at part load is accurately predicted with slight deviations towards the draft tube wall. Applying the kϵ turbulence model does not yield a clear improving trend with commercial code but even negatively affects the computed results with FOAM. This can be lead back to its underlying numerics, which is not able to capture complex flow structures and attached flow regimes in an accurate manner. For this reason, a high level turbulence model like the Reynolds Stress Model (RSM) should be used instead, decreasing the influence of turbulence modeling and providing improved results. In order to reduce the existing deviations between numerics and experimental data in the the near-wall region, a grid refinement should be applied, resolving the physics in the boundary layer without using a standard wall function. Comparing the computed velocity components obtained with either solver, commercial code yields a slightly higher correspondence to the measurements - especially near the runner hub at BEP and HL, where vortex formations are not well predicted by FOAM. Nevertheless, the observed velocity components using FOAM show an appropriate accordance with the experimental data too.

The numerical results obtained with commercial code are less influenced by varying turbulence models and physical models than those computed with FOAM, which can be lead back to the underlying numerics, the implemented damping functions and smoothing algorithms. Focusing on FOAM, there are still differences concerning accuracy and numerical robustness between mixing-plane and the frozen-rotor coupling method: Using mixing-plane needs more computational time to reach a well converged state and the accuracy of the computed results responds more in a sensitive way to changes in convection-specific interpolation schemes. Nevertheless, FOAM is a reasonable alternative to commercial code that makes it possible to adequately predict integral quantities and even values of local parameters under steady operating conditions at part load, best efficiency point and high load.

6. Nomenclature

Symbol	Definition	Symbol	Definition
BEP	Best efficiency point	H	Head (m)
HL	High load	Q	Volumetric flow rate (m^3/s)

Symbol	Definition	Symbol	Definition
PL	Part load	n	Rotational speed $(1/s)$
OP	Operating point	α	Guide vane angle (deg)
DT	Draft tube domain	β	Incidence angle (deg)
GV	Guide vane domain	η	Efficiency (%)
RN	Runner domain	T	Runner shaft torque (Nm)
SC	Spiral case domain	ρ	Density (kg/m^3)
SV	Stay vane domain	I	Turbulent intensity (-)
LDA	Laser Doppler anemometry	l_t	Turbulent mixing length (m)
FR	Frozen-rotor	c_θ	Circumferential velocity (m/s)
MP	Mixing-plane	c_w	Axial velocity (m/s)
GCI	Grid convergence index	r	Radius (m)
h_i	Grid refinement index	y^+	Dimensionless wall distance (-)
CC	Commercial code	Δp_{rel}	Relative pressure deviation (%)
DT11, DT21, P42, P71, S51, VL01	Pressure sensors	$\Delta \eta_{rel}$	Relative efficiency deviation (%)

7. References

[1] H. Keck, M. Sick: Thirty Years of Numerical Flow Simulation in Hydraulic Turbomachines, Acta Mechanica, 201, pp.211-229 , 2008
[2] OpenFOAM Foundation: OpenFOAM Release History, Retrieved October 23, 2014, from `http://www.openfoam.org/download/history.php`
[3] Sig Turbomachinery, Retrieved October 23, 2014, from `http://openfoamwiki.net/index.php/Sig_Turbomachinery`
[4] O. Bounous: Studies of the ERCOFTAC conical diffuser with openFOAM., Department of Applied Mechanics Chalmers University of technology, Gteborg, Sweden, 2008
[5] O. Petit et al.: The ERCOFTAC Centrifugal Pump OpenFOAM Case-Study, In 3rd IAHR International Meeting of the Workgroup of Cavitation and Dynamic Problems in Hydraulic Machinery and Systems, pages 523-532, Brno, Czech Republic, October 2009
[6] H. Nilsson et al.: The OpenFOAM Turbomachinery working-group, and conclusions from the Turbomachinery session of the third OpenFOAM workshop., IAHR: 24th Symposium on Hydraulic Machinery and Systems, Foz do Iguassu, Brazil. 2008
[7] Sig Turbomachinery and Meetings, Retrieved October 23, 2014, from `http://openfoamwiki.net/index.php/Sig_Turbomachinery_/_Meetings`
[8] M. Beaudouin, H. Jasak: Development of a General Grid Interface for turbomachinery simulations with OpenFOAM, Open Source CFD International Conference, November 2008
[9] H. Jasak, M. Beaudoin: OpenFOAM TURBO TOOLS: FROM GENERAL PURPOSE CFD TO TURBOMACHINERY SIMULATIONS, Joint Fluids Engineering Conference, 2011
[10] OpenFOAM extensions, from `http://sourceforge.net/p/openfoam-extend/foam-extend-3.1/ci/master/tree/ReleaseNotes.txt`, 2014
[11] M. Page et al.: Steady-state Capabilities for Hydroturbines with OpenFOAM, International Journal of Fluid Machinery and Systems, 4(1):160-170, Jan-Mar 2011
[12] M. Karlsson et al.: Numerical estimation of torsional dynamic coefficients of a hydraulic turbine, International Journal of Rotating Machinery, 2009
[13] H. Nilsson: Evaluation of OpenFOAM for CFD of turbulent flow in water turbines., IAHR 2006

[14] H. Nilsson: Experiences with OpenFOAM for water turbine applications. Proceedings of the 1st OpenFOAM International Conference, 26-27 November 2007
[15] H. Nilsson: Some experiences on the accuracy and parallel performance of OpenFOAM for CFD in water turbines." Applied Parallel Computing. State of the Art in Scientific Computing. Springer Berlin Heidelberg, 2007. 168-176.
[16] Ch. Trivedi et. al: Experimental and Numerical Studies for a High Head Francis Turbine at Several Operating Points, Journal of Fluids Engineering, Vol. 135/111102-1 , 2013
[17] R. Moritz: Transient CFD-analysis of a high head Francis turbine., 2014
[18] Francis 99 Workshop, from `http://www.ltu.se/research/subjects/Stromningslara/Konferenser/Francis-99/Test-Case-1.111520`, 2014
[19] L.F. Richardson, J.A. Gaunt: The deferred approach to the limit. Philosophical Transactions of the Royal Society of London. Series A, Containing Papers of a Mathematical or Physical Character, 226, 1927
[20] I. B. Celik et al.: Procedure for Estimation and Reporting of Uncertainty Due to Discretization in CFD Applications, Journal of Fluids Engineering, 078001-1, Vol 130, July 2008
[21] P. J. Roache: Verification and Validation in Computational Science and Engineering, Hermosa publishers, Albuquerque, NM, 1998.